Synthesis, Design, and Synchronization Analysis of Coupled Linear Electrical Networks

Karlheinz Ochs*, Dennis Michaelis*, Enver Solan*, Petro Feketa†, Alexander Schaum†, and Thomas Meurer†

*Ruhr-University Bochum
Chair of Digital Communication Systems
Bochum, Germany
Email: {karlheinz.ochs, dennis.michaelis, ever.solan}@rub.de

†Kiel-University
Chair of Automatic Control
Kiel, Germany
Email: {pf, alsc, tm}@tf.uni-kiel.de

***Index Terms*—synchronization, electrical synthesis, Chua's circuit, diffusive coupling, circuit theory.**

***Abstract*—Synchronization has been associated with fundamental brain functions, especially learning behavior. Electrical circuits are candidates to mimic the tremendous information processing ability of simple brain structures due to their inherent massive parallelism. This paper gives an electrical interpretation of synchronization behavior in linear, identical subsystems with diffusive couplings. We consider a general linear state-space model for which we synthesize a minimal, generic electrical circuit. A conductance models the couplings between subsystems to form the overall electrical system. To investigate the synchronization behavior, we show how a beneficial placement of transformers decouples the overall circuit and consequently obtain many smaller circuits that are easier to examine. It is shown that the asymptotic stability in these decoupled circuits leads to a vanishing synchronization error over time. Based on this observation, we are able to formulate a synchronization condition that is entirely dependent on electrical quantities. One benefit, among others, is that by the notion of passivity, the asymptotic stability in some electrical circuits becomes evident without any further calculation. Lastly, we apply these insights to a network of interconnected Chua circuits mimicking neuron populations and their synaptic coupling structure. We investigate different topologies, such as a two ring-topology with a bridge-synapse connection.**

I. Introduction

Synchronization is a hot topic in research today, especially in the context of artificial intelligence and neural networks. It is of interest for a variety of different applications. For example, in order to understand several cognitive functions in the brain, such as perceived visual signal processing [1], processing sensor information [2], event prediction [3], motor control [4], and gait patterns [5]. It has also been extensively investigated in the field of automatic control where it is applicable, among others, to autonomous vehicle platoons [6] and in the context of oscillators. For example, RLC-coupled van der Pol oscillators [7] and inductively-coupled chaotic oscillators [8] have both been investigated in a ring topology. Other prominent oscillators examples include the Kuramoto model [9], [10] or the Chua circuit [11], [12]. The latter is a third-order, minimal electrical circuit that is of particular interest due to its chaotic behavior. Its application examples include music compositions [13], evolution of natural languages [14], secure wireless [15], optical laser communication [16], but most importantly in the context of this work simulations of brain dynamics [17]. Recently, a distributed control scheme was established to synchronize two Chua oscillators in a network without direct interconnection [18].

In order for subsystems to synchronize, they must be able to interchange information about some or all of their states through a coupling network. Besides the particular coupling elements, the interconnection topology plays an important role and has been extensively studied in the context of neural networks [19], [20]. While synchrony is generally desired in neural networks because it is associated with memorizing and learning [21], excessive synchrony can yield to neurological diseases, such as essential tremor [22], epilepsy [23] or Parkinson's disease [24]. It is therefore desirable to establish an easy to check synchronization condition.

Electrical circuits in general are known to perform computing tasks very efficiently due to their inherent massive parallelism and therefore are promising candidates to solve complex tasks [25]–[27]. This is especially beneficial when large setups are investigated, e.g. artificial neural networks. Additionally, electrical circuits are in general easy to mass-produce, cost efficient and can be realized in nanoscale integrated circuits. However, the general synthesis of an electrical circuit is not trivial, but has for example been done to mimic an amoeba's ability to anticipate patterns [28], [29]. Additionally, once a circuit realization is established, approaches like the wave digital concept [30], [31] can be exploited to derive highly flexible software emulators, as it has been done in the context of resistors with a memory [32], [33]. Since the resulting emulator enables parameter manipulation during runtime, in-operando optimization and parameter fitting can be utilized to

work towards possible hardware realizations [34].

The goal of this work is to obtain an electrical interpretation of the synchronization condition known from automatic control for linear identical subsystems with linear, diffusive coupling. This requires synthesizing an electrical circuit of the subsystem and the interconnection network based on a general linear state-space model.

The paper is structured as follows. In Sec. II we synthesize an electrical circuit that describes the dynamics of a single linear state-space model of arbitrary order. The modeling of a connection element, as well as the general network topology description is stated in Sec. III. Accordingly, in Sec. IV multiple of the linear systems described in Sec. II are now interconnected to form the overall system with the goal of synchronization. Consecutively, it is shown in detail which electrical devices can be used to decouple these subsystems for a more compact and structural study. Adding multiple specific transformers to this decoupled setup facilitates an observation of the synchronization error whose asymptotic stability is proven in Sec. V. Lastly, the theory is applied to a set of Chua circuits each mimicking action potential activity of a neuron population on a high abstraction level. After linearization, we apply the methods derived in this work to investigate the synchronization behavior of the setup for various topologies. We verify the theoretical results by simulating our application example with integrated circuit simulation software LTspice. A summary concludes this work.

We understand this manuscript as laying the theoretical groundwork for eletrical interpretation of synchronization and a first step towards understanding how bio-inspired electrical circuits can be utilized for neural synchronization. In short, the main contributions of this work are the following.

(i) A generic approach for synthesis of an electrical circuit for linear state-space models is established
(ii) A procedure to electrically decouple a set of interconnected linear subcircuits with the aim of synchronization is presented
(iii) The asymptotic behavior of the decoupled subsystems then serves the purpose to give information about whether the originally coupled system will synchronize or not. The result is an electrical interpretation of synchronization condition.
(iv) The notion of passivity is helpful to judge the decoupled subsystems' asymptotic behavior easily

II. Subsystem Synthesis

The synthesis part of this work will be separated in the synthesis of the subsystems, which is addressed in this section, and the synthesis of the interconnection network, which is subject to the subsequent section.

We start with a system of $n \in \mathbb{N}$ linear state-space models of order $r \in \mathbb{N}$ with identical dynamics

$$\dot{\boldsymbol{z}}_\mu(t) = \boldsymbol{A}\boldsymbol{z}_\mu(t) + \boldsymbol{b}x_\mu(t), \quad y_\mu(t) = \boldsymbol{c}^T\boldsymbol{z}_\mu(t). \tag{1}$$

where $\boldsymbol{A} \in \mathbb{R}^{r\times r}, \boldsymbol{b}, \boldsymbol{c} \in \mathbb{R}^{r\times 1}$, $\boldsymbol{z}_\mu(t) \in \mathbb{R}^{r\times 1}$, $x_\mu(t), y_\mu(t) \in \mathbb{R}$ and $\mu = 1, \dots, n$. For the sake of readability, we drop the time arguments in the sequel. To synthesize an electrical circuit that mimics the dynamical behavior of (1), we multiply (1) with a constant matrix $C\mathbf{1}_r, C > 0$, where $\mathbf{1}_r$ is the $r \times r$ identity matrix. Next, we decompose $\boldsymbol{A}$ into its symmetric and anti-symmetric parts, $\boldsymbol{G}_\mathrm{s}$ and $\boldsymbol{G}_\mathrm{a}$, respectively. This results in

$$C\dot{\boldsymbol{z}}_\mu + [\boldsymbol{G}_\mathrm{s} + \boldsymbol{G}_\mathrm{a}]\boldsymbol{z}_\mu = \boldsymbol{i}_\mu, \tag{2}$$

with $\boldsymbol{G}_\mathrm{s} = -\frac{C}{2}\left[\boldsymbol{A} + \boldsymbol{A}^T\right]$, $\boldsymbol{G}_\mathrm{a} = -\frac{C}{2}\left[\boldsymbol{A} - \boldsymbol{A}^T\right]$ and $\boldsymbol{i}_\mu = C\boldsymbol{b}x_\mu$, allowing for an electrical circuit synthesis with multiport devices as depicted in Fig. 1.

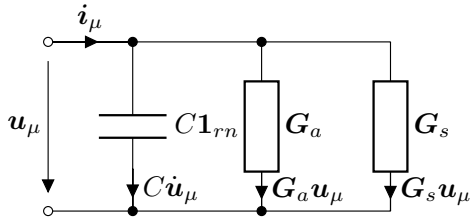

Fig. 1: Electrical synthesis of a general linear state-space model through a parallel interconnection of capacitors and multiport conductances.

When we associate the state vector $\boldsymbol{z}_\mu$ with a set of voltages, this can be synthesized by r capacitors whose currents are described by $\boldsymbol{i}_\mu = C\dot{\boldsymbol{u}}_\mu$, respectively. As the overall current of a subsystem $\boldsymbol{i}_\mu$ is also a summation of multiple summands, this indicates that each electronic device representing one of these summands is interconnected by a Kirchhoff parallel interconnection network. While the r capacitors are straightforward to implement, the question remains on how to realize the conductances $\boldsymbol{G}_\mathrm{s}$ and $\boldsymbol{G}_\mathrm{a}$. In the following, we will show that the key elements in this context are the general multiport gyrator and transformer as shown in Fig. 2, which are discussed here in detail. It is easy to check that the setup of $m \cdot n$ two-port gyrators in Fig. 3 (bottom left) is the realization

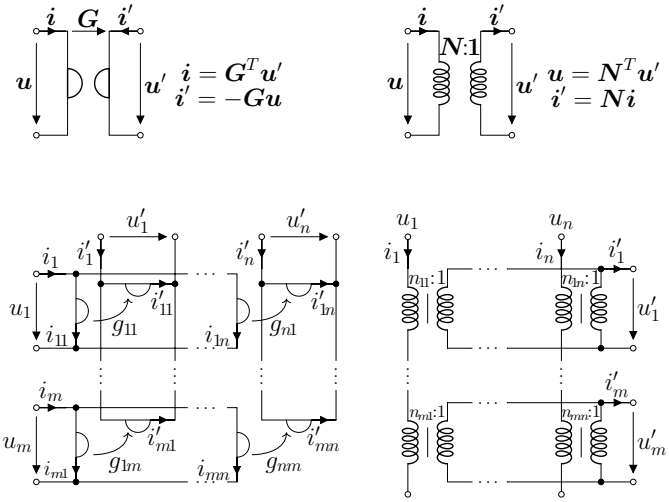

Fig. 2: $m \times n$ multiport gyrator with its scalar realization (left) and $m \times n$ multiport transformer with its scalar realization (right).

of the multiport gyrator shown in Fig. 3 (top left). To do so, we first investigate the two-port gyrator equations

$$i_{\mu\nu} = g_{\nu\mu} u'_\nu, \qquad i'_{\mu\nu} = -g_{\nu\mu} u_\mu. \tag{3}$$

Next, we account for the parallel interconnection network, for which it holds that

$$i_\mu = \sum_{\nu=1}^{n} i_{\mu\nu} = \sum_{\nu=1}^{n} g_{\nu\mu} u'_\nu, \qquad i'_\nu = \sum_{\mu=1}^{n} i'_{\mu\nu} = -\sum_{\mu=1}^{n} g_{\nu\mu} u_\mu. \tag{4}$$

Once (4) is expressed in matrix-vector notation, this yields

$$\boldsymbol{i} = \boldsymbol{G}^T \boldsymbol{u}', \qquad \boldsymbol{i}' = -\boldsymbol{G}\boldsymbol{u}, \tag{5}$$

respectively, which coincides with Fig. 2 (top left). Likewise, the configuration of $m \cdot n$ two-port transformers displayed in Fig. 2 (bottom right) can be checked to fulfill the equations of the multiport transformer of Fig. 2 (top right), which is omitted here for the sake of brevity. In the following, it is explained how the multiport gyrator and transformer are essential in the synthesis of the symmetric and antisymmetric parts of the system matrix $\boldsymbol{A}$.

Asymptotically stable subsystems, which are identifiable by a positive definite symmetric part $\boldsymbol{G}_\mathrm{s}$, are of little interest, as they converge to the trivial solution $\boldsymbol{z}_\mu = \boldsymbol{0}$ and hence synchronize without any requirement of interconnection. Our work therefore focuses on subsystems which are marginally stable or unstable. To synthesize the symmetric part, we utilize the eigenvalue decomposition $\boldsymbol{G}_\mathrm{s} = \boldsymbol{N}_\mathrm{s}^T \boldsymbol{G}_\mathrm{d} \boldsymbol{N}_\mathrm{s}$ where $\boldsymbol{G}_\mathrm{d}$ is a diagonal matrix containing the r real eigenvalues which can be both positive and negative. $\boldsymbol{N}_\mathrm{s}$ is the $r \times r$ eigenmatrix containing the eigenvectors. This enables us to represent the symmetric part by r conductances in conjunction with at most r^2 transformers with transmission ratios taken from the eigenmatrix $\boldsymbol{N}_\mathrm{s}$, see Fig. 3 (left). Note, this approach causes negative eigenvalues to be represented by negative conductance values. For the anti-symmetric part $\boldsymbol{G}_\mathrm{a}$ we utilize the decomposition $\boldsymbol{G}_\mathrm{a} = \boldsymbol{G}_\mathrm{G} - \boldsymbol{G}_\mathrm{G}^T = -\boldsymbol{G}_\mathrm{a}^T$, where $\boldsymbol{G}_\mathrm{G}$ is a strictly lower triangular matrix, as shown in Fig. 3 (right). Consequently, it holds for the antisymmetric part that $\boldsymbol{i}_\mathrm{a} = \boldsymbol{G}_\mathrm{a}\boldsymbol{u} = \boldsymbol{G}_\mathrm{G}\boldsymbol{u} - \boldsymbol{G}_\mathrm{G}^T\boldsymbol{u}$. Starting from (5), this can be achieved by making sure that $\boldsymbol{u} = \boldsymbol{u}'$ and $\boldsymbol{i}_\mathrm{a} = \boldsymbol{i}_\mathrm{G} - \boldsymbol{i}'_\mathrm{G}$, which is attained by interconnecting the multiport transformer as shown in Fig. 3 (right).

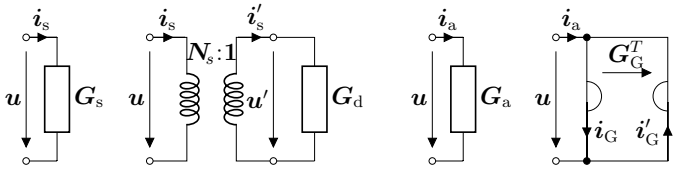

Fig. 3: Conductance matrix $\boldsymbol{G}_\mathrm{s}$, realized by a multiport transformer in combination with a diagonal conductance matrix $\boldsymbol{G}_\mathrm{d}$ (left). Conductance $\boldsymbol{G}_\mathrm{a}$ with its realization by a multiport gyrator in short-circuit configuration (right).

With the details regarding the scalar realization of $\boldsymbol{G}_\mathrm{s}$ and $\boldsymbol{G}_\mathrm{a}$ discussed, we now incorporate the details of Fig. 3 into the general setup of Fig. 1. This yields the electrical circuit of Fig. 4. Note, although we still use the multiport description for reasons of efficient depiction, all underlying one-port realizations have been discussed above. Consequently, Fig. 4 contains all these information. It is worth noting that the complementary electrical quantities $\boldsymbol{u}_\mu$ and $\boldsymbol{i}_\mu$ at the port are the input and output signals.

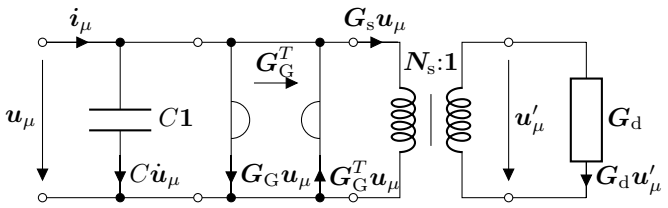

Fig. 4: Detailed multiport depiction of the electrical circuit in Fig. 1 that together with the multiport gyrator and transformer of Fig. 2 efficiently represents the underlying one-port realization.

III. Coupling Network Synthesis

To achieve synchronization in unstable subsystems, coupling between the subsystems is essential. Throughout this work we assume linear diffusive coupling with constant coupling strengths. From a graph theoretical point of view, the subsystems can be associated with a set of vertices, where the subsystem μ is represented by vertex a_μ. Then, edge $b_\kappa = (a_\mu, a_\nu)$ exists if subsystems μ and ν are connected. Note that to capture every connection only once, we choose the direction of all edges such that they originate from the lower indexed subsystem and are directed towards the higher indexed subsystem. Additionally, $\kappa = 1, \ldots, k$, where k is the total number of interconnections in the interconnection network. Specifically, $k = 0$ reflects the case where no subsystems are interconnected and $k = \frac{n[n-1]}{2}$ implies a fully connected topology. With this information, the network is interpreted as a graph and we define the incidence matrix $\boldsymbol{N} \in \mathbb{R}^{n \times k}$, with elements $n_{\mu\kappa}$ of the topology as

$$n_{\mu\kappa} = \begin{cases} +1, & \text{if } b_\kappa = (\cdot, a_\mu), \\ -1, & \text{if } b_\kappa = (a_\mu, \cdot), \\ 0, & \text{otherwise.} \end{cases} \tag{6}$$

In this context, $b_\kappa = (\cdot, a_\mu)$ indicates that edge b_κ originates from an arbitrary vertex and incides at vertex a_μ whereas $b_\kappa = (a_\mu, \cdot)$ indicates that edge b_κ originates from vertex a_μ and incides at an arbitrary vertex. In a circuit description, we assign current $\boldsymbol{i}_\mu$ and voltage $\boldsymbol{u}_\mu$ to subsystem μ, and the currents and voltage between subsystems μ and ν are referenced as $\boldsymbol{j}_{\mu\nu}$ and $\boldsymbol{v}_{\mu\nu}$, respectively. By establishing the Kirchhoff node and mesh equations, we obtain

$$\boldsymbol{v}_{\mu\nu} = \boldsymbol{u}_\mu - \boldsymbol{u}_\nu, \qquad \boldsymbol{i}_\mu = \sum_{\lambda>\mu} \boldsymbol{j}_{\mu\lambda} - \sum_{\lambda<\mu} \boldsymbol{j}_{\lambda\mu}, \tag{7}$$

cf. Fig. 5 (left), with $\boldsymbol{i}_\mu, \boldsymbol{j}_{\mu\nu} \in \mathbb{R}^r$.

Note that $\boldsymbol{v}_{\mu\nu}$ and $\boldsymbol{j}_{\mu\nu}$ which are obtained by differences of $\boldsymbol{u}_\mu$, $\boldsymbol{u}_\nu$ and $\boldsymbol{i}_\mu$, $\boldsymbol{i}_\nu$, cf. (7), are only of interest if subsystems μ and ν are coupled. The orientation of $\boldsymbol{j}_{\mu\nu}$ are chosen such

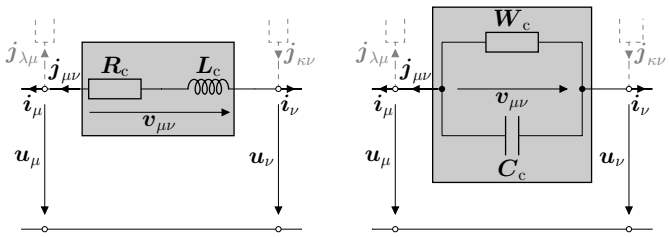

Fig. 5: Electrical circuit of a simple synapse as proposed in [35] (left) and its dual circuit (right).

that the (directed) incidence matrix $\boldsymbol{N}$ describes the relation between the quantities of the subsystems and the quantities of the interconnection network.

The electrical circuit of a simple synapse model as described in [35] is shown in Fig. 5. Its underlying electrical equations are

$$\boldsymbol{v}_{\mu\nu} = -\boldsymbol{R}_\mathrm{c}\boldsymbol{j}_{\mu\nu} - \boldsymbol{L}_\mathrm{c}\dot{\boldsymbol{j}}_{\mu\nu}.$$

However, the input of the synthesized state-space model of Fig. 4 is modeled by a current. Therefore it seems natural to rather investigate the dual circuit of the synaptic model, where the roles of voltage and current are interchanged. This can be seen in the electrical equations for the dual representation as shown Fig. 5 (right), which are

$$\boldsymbol{j}_{\mu\nu} = -\boldsymbol{W}_\mathrm{c}\boldsymbol{v}_{\mu\nu} - \boldsymbol{C}_\mathrm{c}\dot{\boldsymbol{v}}_{\mu\nu}, \tag{8}$$

with $\boldsymbol{W}_\mathrm{c} = W_\mathrm{c}\boldsymbol{b}\boldsymbol{c}^T$ and $\boldsymbol{C}_\mathrm{c} = C_\mathrm{c}\boldsymbol{b}\boldsymbol{c}^T$. For the sake of a more condensed representation, we deploy the vec-operator, where $\mathrm{vec}(\cdot)$ stacks the columns of a matrix on top of one another to form a vector. Now, if we define vectors $\boldsymbol{j} = \mathrm{vec}(\boldsymbol{J}) \in \mathbb{R}^{rk}$ where $\boldsymbol{J} \in \mathbb{R}^{r\times k}$ contains all $\boldsymbol{j}_{\mu\nu}$ column-wise in ascending order and $\boldsymbol{v} = \mathrm{vec}(\boldsymbol{V}) \in \mathbb{R}^{rk}$ with $\boldsymbol{V} \in \mathbb{R}^{r\times k}$ contains all $\boldsymbol{v}_{\mu\nu}$ column-wise in ascending order, we can rewrite (8) with

$$\boldsymbol{v} = \hat{\boldsymbol{N}}^T\boldsymbol{u}, \qquad \boldsymbol{i} = \hat{\boldsymbol{N}}\boldsymbol{j}, \tag{9}$$

where $\boldsymbol{u} = \begin{bmatrix}\boldsymbol{u}_1^T & \dots & \boldsymbol{u}_n^T\end{bmatrix}^T \in \mathbb{R}^{rn}$, $\boldsymbol{i} = \begin{bmatrix}\boldsymbol{i}_1^T & \dots & \boldsymbol{i}_n^T\end{bmatrix}^T \in \mathbb{R}^{rn}$ and $\hat{\boldsymbol{N}} = \boldsymbol{N}\otimes\boldsymbol{1}_r$ with $\boldsymbol{N}$ being the incidence matrix as described in (6) and $\otimes$ denoting the Kronecker product. By looking at the equations of the multiport transformer in Fig. 2, it becomes clear that we can utilize a $\boldsymbol{1} : \hat{\boldsymbol{N}}$-transformer to synthesize (9) as will be shown later. With the vector

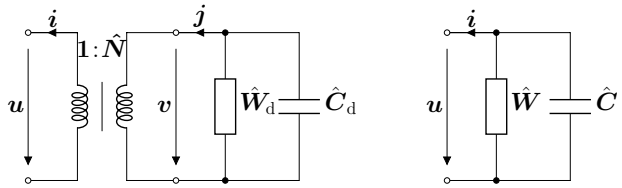

Fig. 6: Multiport interconnection network representation by a transformer whose transmission ratio depends on incidence matrix $\hat{\boldsymbol{N}}$ (left). Effective interconnection multiport representation in instances $\boldsymbol{i}$ and $\boldsymbol{u}$, respectively (right).

descriptions $\boldsymbol{u}, \boldsymbol{i}$ and $\boldsymbol{v}, \boldsymbol{j}$, we rewrite the first part of (8) as

$$\boldsymbol{j} = -\hat{\boldsymbol{W}}_\mathrm{d}\boldsymbol{v} - \hat{\boldsymbol{C}}_\mathrm{d}\dot{\boldsymbol{v}}, \tag{10}$$

with $\hat{\boldsymbol{W}}_\mathrm{d} = \boldsymbol{1}_n\otimes\boldsymbol{W}_\mathrm{c}$ and $\hat{\boldsymbol{C}}_\mathrm{d} = \boldsymbol{1}_n\otimes\boldsymbol{C}_\mathrm{c}$. The according circuit is shown in Fig. 6 (left). Together with (9), the device equation can be written in terms of the vertex currents and voltages

$$\begin{aligned}\boldsymbol{i} &= -\hat{\boldsymbol{N}}\hat{\boldsymbol{W}}_\mathrm{d}\hat{\boldsymbol{N}}^T\boldsymbol{u} - \hat{\boldsymbol{N}}\hat{\boldsymbol{C}}_\mathrm{d}\hat{\boldsymbol{N}}^T\dot{\boldsymbol{u}}\\ &= -[\boldsymbol{N}\otimes\boldsymbol{1}_r][\boldsymbol{1}_n\otimes\boldsymbol{W}_\mathrm{c}][\boldsymbol{N}^T\otimes\boldsymbol{1}_r]\boldsymbol{u}\\ &\quad -[\boldsymbol{N}\otimes\boldsymbol{1}_r][\boldsymbol{1}_n\otimes\boldsymbol{C}_\mathrm{c}][\boldsymbol{N}^T\otimes\boldsymbol{1}_r]\dot{\boldsymbol{u}}.\end{aligned}$$

By utilizing the definition of the Laplace matrix $\boldsymbol{L} = \boldsymbol{N}\boldsymbol{N}^T \in \mathbb{R}^{n\times n}$ and the properties of the Kronecker product, we obtain the compact relationship

$$\begin{aligned}\boldsymbol{i} &= -[\boldsymbol{N}\boldsymbol{N}^T\otimes\boldsymbol{W}_\mathrm{c}]\boldsymbol{u} - [\boldsymbol{N}\boldsymbol{N}^T\otimes\boldsymbol{C}_\mathrm{c}]\dot{\boldsymbol{u}}\\ &= -[\boldsymbol{L}\otimes\boldsymbol{W}_\mathrm{c}]\boldsymbol{u} - [\boldsymbol{L}\otimes\boldsymbol{C}_\mathrm{c}]\dot{\boldsymbol{u}}\\ &= -\hat{\boldsymbol{W}}\boldsymbol{u} - \hat{\boldsymbol{C}}\dot{\boldsymbol{u}},\end{aligned} \tag{11}$$

with $\hat{\boldsymbol{W}} = \boldsymbol{L}\otimes\boldsymbol{W}_\mathrm{c}$ and $\hat{\boldsymbol{C}} = \boldsymbol{L}\otimes\boldsymbol{C}_\mathrm{c}$. The expressions in (11) result in the interconnection network description as shown in the right-hand side of Fig. 6.

IV. Coupled System

Combining the insights from Figs. 1 and 6, we can describe the multiport coupled system as shown in Fig. 7. The equation to describe the overall system is

$$\left[C\boldsymbol{1}_r + \hat{\boldsymbol{C}}\right]\dot{\boldsymbol{u}} + \left[\hat{\boldsymbol{G}}_\mathrm{s} + \hat{\boldsymbol{G}}_\mathrm{a} + \hat{\boldsymbol{W}}\right]\boldsymbol{u} = \boldsymbol{0}, \tag{12}$$

with $\hat{\boldsymbol{G}}_\mathrm{s} = \boldsymbol{1}_n\otimes\boldsymbol{G}_\mathrm{s}$ and $\hat{\boldsymbol{G}}_\mathrm{a} = \boldsymbol{1}_n\otimes\boldsymbol{G}_\mathrm{a}$.

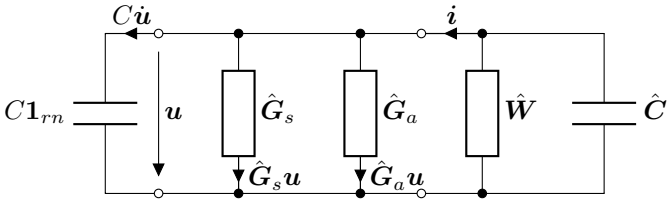

Fig. 7: Coupled overall system description, cf. Figs. 1 and 6.

Note that this description of the system still incorporates coupled subsystems, since $\hat{\boldsymbol{W}}$ is not block diagonal. In the following, we will describe on how to arrive at decoupled electrical circuits that will be used later on for determining the synchronization condition by block diagonalizing $\hat{\boldsymbol{W}}$ with multiport transformers.

Since the matrix

$$\hat{\boldsymbol{W}} = \hat{\boldsymbol{N}}\hat{\boldsymbol{W}}_\mathrm{d}\hat{\boldsymbol{N}}^T = \left[\hat{\boldsymbol{N}}\hat{\boldsymbol{W}}_\mathrm{d}\hat{\boldsymbol{N}}^T\right]^T = \hat{\boldsymbol{W}}^T \tag{13}$$

is symmetric, there always exists an eigenvalue decomposition of $\hat{\boldsymbol{W}}$ with eigenmatrix $\hat{\boldsymbol{T}} = \boldsymbol{T}\otimes\boldsymbol{1}_r$, $\boldsymbol{T} \in \mathbb{N}^{n\times n}$, such that $\hat{\boldsymbol{T}}$ is orthogonal. Now, we elaborate on how to electrically diagonalize the interconnection network matrix $\hat{\boldsymbol{W}}$ and hence decouple the subsystems. We start by showing that the necessary steps to achieve the decoupling do not alter the structure of the subsystems.

Remark 1. *A state transformation with transformation matrix $\hat{\boldsymbol{T}}$ can electrically be realized by a $\boldsymbol{1} : \hat{\boldsymbol{T}}$ and a $\hat{\boldsymbol{T}} : \boldsymbol{1}$ multiport transformers if and only if $\hat{\boldsymbol{T}}^T\hat{\boldsymbol{T}} = \boldsymbol{1}$.*

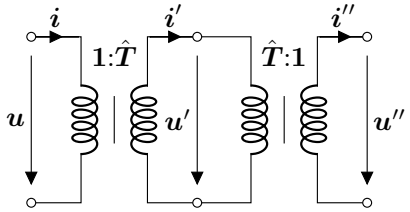

Fig. 8: Two multiport transformers with transformation ratios $\mathbf{1} : \hat{\boldsymbol{T}}$ and $\hat{\boldsymbol{T}} : \mathbf{1}$ cascaded to form a neutral element as $\boldsymbol{u} = \boldsymbol{u}''$ and $\boldsymbol{i} = \boldsymbol{i}''$.

First, by interconnecting a $\mathbf{1} : \hat{\boldsymbol{T}}$ transformer and a $\hat{\boldsymbol{T}} : \mathbf{1}$ transformer, as shown in Fig. 8, the resulting underlying equations are

$$\begin{aligned} \boldsymbol{u}' &= \hat{\boldsymbol{T}}^T \boldsymbol{u}, \quad \boldsymbol{u}' = \hat{\boldsymbol{T}}^T \boldsymbol{u}'', \\ \boldsymbol{i} &= \hat{\boldsymbol{T}} \boldsymbol{i}', \quad \boldsymbol{i}'' = \hat{\boldsymbol{T}} \boldsymbol{i}'. \end{aligned} \tag{14}$$

Since $\hat{\boldsymbol{T}}$ is invertible, this concludes that $\boldsymbol{u} = \boldsymbol{u}''$ and $\boldsymbol{i} = \boldsymbol{i}''$, indicating that it is indeed a neutral element. To decouple the subsystems, we place it in between the subsystems and its input, as displayed in Fig. 9.

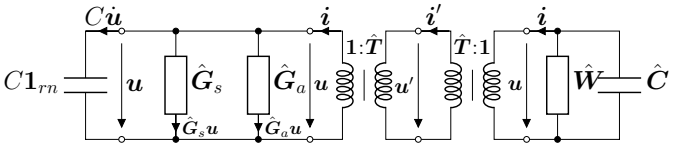

Fig. 9: Neutral cascade of Fig. 8 inserted between subsystems and coupling network. Expressing this setup in instances $\boldsymbol{u}'$, $\boldsymbol{i}'$ will lead to a decoupled overall system.

Remark 2. *Given matrices of appropriate dimensions, an arbitrary square matrix $\hat{\boldsymbol{X}} = \mathbf{1}_n \otimes \boldsymbol{X}$ remains invariant to a regular state transformation with transformation matrix $\hat{\boldsymbol{T}} = \boldsymbol{T} \otimes \mathbf{1}_r$. This becomes evident by the properties of the Kronecker product which yield*

$$\begin{aligned} \hat{\boldsymbol{T}}^{-1} \hat{\boldsymbol{X}} \hat{\boldsymbol{T}} &= [\boldsymbol{T}^{-1} \otimes \mathbf{1}_r][\mathbf{1}_n \otimes \boldsymbol{X}][\boldsymbol{T} \otimes \mathbf{1}_r] \\ &= \boldsymbol{T}^{-1}\boldsymbol{T} \otimes \boldsymbol{X} = \mathbf{1}_n \otimes \boldsymbol{X} = \hat{\boldsymbol{X}}. \end{aligned}$$

The subsystem differential equation

$$C\dot{\boldsymbol{u}} + [\hat{\boldsymbol{G}}_\mathrm{s} + \hat{\boldsymbol{G}}_\mathrm{a}]\boldsymbol{u} = \boldsymbol{i}, \tag{15}$$

together with the left-hand transformer equations

$$\boldsymbol{u}' = \hat{\boldsymbol{T}}^T \boldsymbol{u}, \quad \boldsymbol{i} = \hat{\boldsymbol{T}} \boldsymbol{i}', \tag{16}$$

leads to $C\hat{\boldsymbol{T}}^T \hat{\boldsymbol{T}} \dot{\boldsymbol{u}}' + \hat{\boldsymbol{T}}^T [\hat{\boldsymbol{G}}_\mathrm{s} + \hat{\boldsymbol{G}}_\mathrm{a}] \hat{\boldsymbol{T}} \boldsymbol{u}' = \boldsymbol{i}'$, and hence to

$$C\dot{\boldsymbol{u}}' + [\hat{\boldsymbol{G}}_\mathrm{s} + \hat{\boldsymbol{G}}_\mathrm{a}]\boldsymbol{u}' = \boldsymbol{i}', \tag{17}$$

as explained in Remark 2. Note, (17) indicates that the structure of the subsystems remains invariant with respect to the state transformation. The interconnection network

$$\boldsymbol{i} = -\hat{\boldsymbol{W}}\boldsymbol{u} - \hat{\boldsymbol{C}}\dot{\boldsymbol{u}}, \tag{18}$$

and the right-hand side transformer equation (16) results in

$$\begin{aligned} \boldsymbol{i}' &= -\hat{\boldsymbol{T}}^T \hat{\boldsymbol{W}} \hat{\boldsymbol{T}} \boldsymbol{u}' - \hat{\boldsymbol{T}}^T \hat{\boldsymbol{C}} \hat{\boldsymbol{T}} \dot{\boldsymbol{u}}' \\ &= -[\boldsymbol{T}^T \boldsymbol{L} \boldsymbol{T} \otimes \boldsymbol{W}_\mathrm{c}]\boldsymbol{u}' - [\boldsymbol{T}^T \boldsymbol{L} \boldsymbol{T} \otimes \boldsymbol{C}_\mathrm{c}]\dot{\boldsymbol{u}}' \\ &= -[\boldsymbol{\Lambda}_L \otimes \boldsymbol{W}_\mathrm{c}]\boldsymbol{u}' - [\boldsymbol{\Lambda}_L \otimes \boldsymbol{C}_\mathrm{c}]\dot{\boldsymbol{u}}', \end{aligned} \tag{19}$$

where $\boldsymbol{T}$ is chosen as the eigenmatrix of $\boldsymbol{L}$, such that $\boldsymbol{\Lambda}_L = \boldsymbol{T}^T \boldsymbol{L} \boldsymbol{T} = \operatorname{diag}\{\lambda_\mu\{\boldsymbol{L}\}\}$ contains all eigenvalues of $\boldsymbol{L}$ in ascending order $\lambda_1\{\boldsymbol{L}\} = 0 \leq \cdots \leq \lambda_n\{\boldsymbol{L}\}$ on its main diagonal. If $\boldsymbol{T}$ is chosen as the eigenmatrix of $\boldsymbol{L}$, then $\hat{\boldsymbol{T}} = \boldsymbol{T} \otimes \mathbf{1}_r$ block-diagonalizes $\hat{\boldsymbol{W}}$ and $\hat{\boldsymbol{C}}$ simultaneously, as can be seen in (19). For the electrical circuit, this means that we decouple the interconnection network without structurally affecting the independent subsystems, as displayed in Fig. 10 (top). The underlying equation is

$$[C\mathbf{1}_r + \lambda_\mu\{\boldsymbol{L}\}\boldsymbol{C}_\mathrm{c}]\,\dot{\boldsymbol{u}}'_\mu + [\boldsymbol{G}_\mathrm{s} + \boldsymbol{G}_\mathrm{a} + \lambda_\mu\{\boldsymbol{L}\}\boldsymbol{W}_\mathrm{c}]\,\boldsymbol{u}'_\mu = \mathbf{0}. \tag{20}$$

Its condensed representation, cf. Fig. 10 (bottom), beautifully highlights the structural simplicity of our approach. In the following it will be shown how the asymptotic stability of these decoupled subsystems $\mathcal{N}'_\mu$, which is significantly easier to examine compared to the coupled overall system, is the determining factor in whether synchronization is achieved or not.

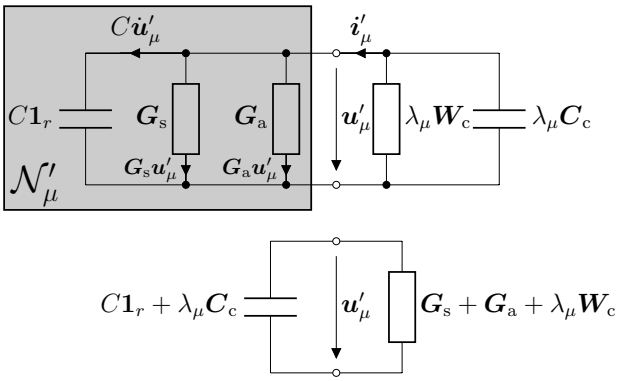

Fig. 10: Decoupled systems $\mathcal{N}'_\mu$ in the quantities $\boldsymbol{u}'_\mu$, $\boldsymbol{i}'_\mu$ after the transformation (top). Its condensed representation (bottom) truly reveals the simple structure.

V. Asymptotic Stability of Error Dynamics and Synchronization Condition

A. Error System and Synchronization Condition

Before the derivation of the synchronization error, we highlight important features of the transformation matrix $\boldsymbol{T}$ in conjunction with the incidence matrix $\boldsymbol{N}$. Specifically, as it is known that the row and column sum of the Laplace matrix $\boldsymbol{L}$ is zero, and its eigenvector $\boldsymbol{t}_1 = \frac{1}{\sqrt{n}}\mathbb{1}_n$ is associated with the eigenvalue $\lambda_1\{\boldsymbol{L}\} = 0$, where $\mathbb{1}_n$ is the $n \times 1$ all one vector [36]. Additionally, as the column sum of the incidence matrix $\boldsymbol{N}$ is always zero, it holds that

$$\begin{aligned} \boldsymbol{N}^T\boldsymbol{T} &= \boldsymbol{N}^T \left[\tfrac{1}{\sqrt{n}}\mathbb{1}_n \,\middle|\, \boldsymbol{t}_2 \quad \dots \quad \boldsymbol{t}_n\right] \\ &= \left[\mathbf{0} \,\middle|\, \boldsymbol{N}^T\boldsymbol{t}_2 \quad \dots \quad \boldsymbol{N}^T\boldsymbol{t}_n\right] = \left[\mathbf{0} \,\middle|\, \boldsymbol{E}\right], \end{aligned} \tag{21}$$

with $\boldsymbol{E} = [\boldsymbol{N}^T\boldsymbol{t}_2 \ \dots \ \boldsymbol{N}^T\boldsymbol{t}_n] \in \mathbb{R}^{k\times[n-1]}$ and $\boldsymbol{t}_\mu$ being the μ-th column of $\boldsymbol{T}$. To monitor the synchronization errors, we use the incidence matrix to obtain the synchronization errors from the transformed states $\boldsymbol{u}'$ (16) by

$$\boldsymbol{e} = \hat{\boldsymbol{N}}^T\boldsymbol{u} = \hat{\boldsymbol{N}}^T\hat{\boldsymbol{T}}\hat{\boldsymbol{T}}^T\boldsymbol{u} = [\boldsymbol{N}^T\boldsymbol{T}\otimes\mathbf{1}_n]\boldsymbol{u}'. \tag{22}$$

Together with (21) we obtain

$$\boldsymbol{e} = \begin{bmatrix}\boldsymbol{e}_1\\ \vdots\\ \boldsymbol{e}_k\end{bmatrix} = \hat{\boldsymbol{E}}\begin{bmatrix}\boldsymbol{u}_2'\\ \vdots\\ \boldsymbol{u}_n'\end{bmatrix} = \begin{bmatrix}\hat{\boldsymbol{E}}_{12} & \dots & \hat{\boldsymbol{E}}_{1n}\\ \vdots & \ddots & \vdots\\ \hat{\boldsymbol{E}}_{k2} & \dots & \hat{\boldsymbol{E}}_{kn}\end{bmatrix}\begin{bmatrix}\boldsymbol{u}_2'\\ \vdots\\ \boldsymbol{u}_n'\end{bmatrix}, \tag{23}$$

with $\hat{\boldsymbol{E}} = \boldsymbol{E}\otimes\mathbf{1}_r$, $\hat{\boldsymbol{E}}_{\kappa\mu} \in \mathbb{R}^{r\times r}$, $\kappa = 1,\dots,k$ and $\mu = 2,\dots,n$. The synchronization errors of (23) are synthesized by the circuit shown in Fig. 11.

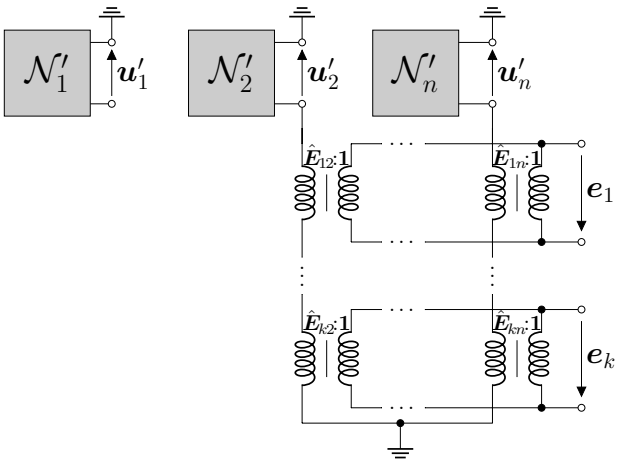

Fig. 11: Synchronization error system $\boldsymbol{e}_1,\dots,\boldsymbol{e}_k$ obtained by the decoupled subsystems $\mathcal{N}_2',\dots\mathcal{N}_n'$.

Theorem 1. *Consider the overall system of of Fig. 7 and let the interconnection topology contain at least one spanning tree. Then, the synchronization errors $\boldsymbol{e}$ vanish, i.e. $\lim_{t\to\infty}\boldsymbol{e} = \mathbf{0}$, if and only if*

$$\lim_{t\to\infty}\begin{bmatrix}\boldsymbol{u}_2'\\ \vdots\\ \boldsymbol{u}_n'\end{bmatrix} = \mathbf{0}. \tag{24}$$

The common asymptotic synchronization trajectory is then given by $\boldsymbol{u}_1'$.

Proof. Since an overall system with n subsystems is investigated, there exist exactly $n-1$ independent synchronization errors amongst the k synchronization errors in $\boldsymbol{e}$ in (23) if $\operatorname{rank}(\hat{\boldsymbol{E}}) = r[n-1]$. Thus, the null-space of $\hat{\boldsymbol{E}}$ consists only of the zero vector and consequently $\boldsymbol{e} = \mathbf{0}$ implies $\boldsymbol{u}_2' = \boldsymbol{u}_n' = \mathbf{0}$. Together with (21) we further investigate the rank of $\boldsymbol{E}$

$$\begin{aligned}\operatorname{rank}(\hat{\boldsymbol{E}}) &= \operatorname{rank}(\boldsymbol{E})\operatorname{rank}(\mathbf{1}_r)\\ &= \min\left\{\operatorname{rank}(\boldsymbol{N}), \operatorname{rank}\left([\boldsymbol{t}_2\dots\boldsymbol{t}_n]\right)\right\} r\\ &= \operatorname{rank}(\boldsymbol{N})\, r,\end{aligned} \tag{25}$$

because $\boldsymbol{T}$ is invertible, consequently has $\operatorname{rank}(\boldsymbol{T}) = n$ and therefore $\operatorname{rank}\left([\boldsymbol{t}_2\dots\boldsymbol{t}_n]\right) = n-1$ while the rank of $\boldsymbol{N}$ is $\operatorname{rank}(\boldsymbol{N}) \le n-1$. The rank of $\boldsymbol{N}$ is equal to $n-1$ if and only if $\lambda_2\{\boldsymbol{L}\} \neq 0$, which is synonymous with stating that $\boldsymbol{N}$ belongs to a topology containing at least one spanning tree [36]. Given such a topology, by (25), the asymptotic stability of the decoupled subsystems $\mathcal{N}_2',\dots,\mathcal{N}_n'$ of Fig. 10 is equivalent to the asymptotic stability of synchronization errors

$$\lim_{t\to\infty}\begin{bmatrix}\boldsymbol{u}_2'\\ \vdots\\ \boldsymbol{u}_n'\end{bmatrix} = \mathbf{0} \quad\Leftrightarrow\quad \lim_{t\to\infty}\begin{bmatrix}\boldsymbol{e}_1\\ \vdots\\ \boldsymbol{e}_k\end{bmatrix} = \mathbf{0}. \tag{26}$$

After proving the condition for the asymptotic stability of the synchronization error, we now focus on the common synchronization trajectory. The common asymptotic synchronization trajectory can be determined by the single non-coupled system $\mathcal{N}_1'$, which is structurally identical to the subsystems $\mathcal{N}_1,\dots,\mathcal{N}_n$. Calculating $\boldsymbol{u}_1'$, we obtain

$$\begin{aligned}\hat{\boldsymbol{T}}^T\boldsymbol{u} &= \begin{bmatrix}\frac{1}{\sqrt{n}}\mathbb{1}_n^T\otimes\mathbf{1}_r\\ \hline \boldsymbol{t}_2^T\otimes\mathbf{1}_r\\ \vdots\\ \boldsymbol{t}_n^T\otimes\mathbf{1}_r\end{bmatrix}\boldsymbol{u} = \begin{bmatrix}\frac{1}{\sqrt{n}}\sum_{\mu=1}^n\boldsymbol{u}_\mu\\ \hline *\end{bmatrix}\\ &= \left[\begin{array}{c|ccc}\boldsymbol{u}_1'^T & \boldsymbol{u}_2'^T & \dots & \boldsymbol{u}_n'^T\end{array}\right]^T = \boldsymbol{u}'.\end{aligned} \tag{27}$$

By (27), it can be seen that the initial condition $\boldsymbol{u}_{10}'$ of $\mathcal{N}_1'$, is determined by the mean over all initial conditions $\boldsymbol{u}_{\mu 0}$ of all subsystems, resulting in $\boldsymbol{u}_{10}' = \frac{1}{n}\sum_{\mu=1}^n\boldsymbol{u}_{\mu 0}$. Note that the coupling does not stabilize the subsystems, it only makes the synchronization errors $\boldsymbol{e}_1,\dots,\boldsymbol{e}_k$ asymptotically stable. □

A formal procedure to check if subsystems $\mathcal{N}_2',\dots,\mathcal{N}_n'$ are asymptotically stable is mentioned in Theorem 2.

Theorem 2. *Let the interconnection topology contain at least one spanning tree, then the systems $\mathcal{N}_2',\dots,\mathcal{N}_n'$ of Fig. 10 and (20) are asymptotically stable if and only if all of the following matrices' symmetric parts are positive definite:*

$$\left[C\mathbf{1}_r + \lambda_\mu\{\boldsymbol{L}\}\boldsymbol{C}_\mathrm{c}\right]^{-1}\left[\boldsymbol{G}_\mathrm{s} + \boldsymbol{G}_\mathrm{a} + \lambda_\mu\{\boldsymbol{L}\}\boldsymbol{W}_\mathrm{c}\right] > \mathbf{0}, \tag{28}$$

$\mu = 2,\dots,n$.

Since $\boldsymbol{G}_\mathrm{s}$ is typically not a positive definite matrix, $\boldsymbol{W}_\mathrm{c}$ and $\boldsymbol{C}_\mathrm{c}$ must be chosen such that (28) is satisfied for any topology $\boldsymbol{L}$ containing at least one spanning tree to synchronize all subsystems on a common trajectory. Note that by the matrix inversion lemma, the inverse is

$$\left[C\mathbf{1}_r + \lambda_\mu\{\boldsymbol{L}\}\boldsymbol{C}_\mathrm{c}\right]^{-1} = \frac{1}{C}\left[\mathbf{1}_r - \frac{\lambda_\mu^*\boldsymbol{b}\boldsymbol{c}^T}{1+\lambda_\mu^*\boldsymbol{c}^T\boldsymbol{b}}\right],$$

which exists only if $1+\lambda_\mu^*\boldsymbol{c}^T\boldsymbol{b} \neq 0$, with $\lambda_\mu^* = \lambda_\mu\{\boldsymbol{L}\}\frac{C_\mathrm{c}}{C}$.

However, there are also ways to check the asymptotic stability of a circuit without determination of the positive definiteness of a matrix (and consequently without calculating an inverse of a matrix). For example, if the circuit synthesis of subsystems $\mathcal{N}_2',\dots,\mathcal{N}_n'$ only contains passive elements, the overall circuit is passive, its equilibrium $\mathbf{0}$ is stable and it is often times easy to check its asymptotic stability by network theoretic methods. This insight is exploited in the following section. Note that for a purely resistive coupling element, the results presented in Theorem 1 and Theorem 2 coincide with the system theoretic results known in the literature [37].

VI. Application Example: Neuron Population Synchronization by linearized Chua Circuit

In the following we will apply the concept to a set of oscillators which mimic neuronal activity (superposition of action potential) of neuron populations. When investigating large amounts of neurons within a neuron population, some sort of abstraction is helpful. Here, the chaotic behavior of a Chua circuit accounts for the abstraction of the neuronal activity within a neuron population. While a direct biological interpretation is lost in the process, it serves the purpose for analysis on a higher level. The goal of this application example is a first step towards an understanding of neural synchronization with manageable methods. For this reason, a simple conductance accounts for the synaptic coupling strength of the purely electrical synapse.

Although the derived concept only applies to linear systems, it gives us an idea how to derive an electrical interpretation of a sufficient synchronization condition in the context of neuronal networks by the means of linearization. Fig. 12 illustrates the outline of the application example and how the concept is deployed. Initially, only a coupling between neuron populations 1 and 3, and 4 and 6 exist, respectively. At $t = T_1$, further couplings form, such that populations 1, 2 and 3, and 4, 5 and 6 each form a ring, respectively. At $t = T_2$ a bridge-synapse-like coupling between populations 2 and 6 connects the two formerly disconnected rings. Every step depicted is listed below in detail.

A. Technical abstraction

Chaotic oscillators have been used in the literature in the context of synchronization in neuronal networks [17], [38]. Chua's circuit [11] is a setup containing the minimal required number of electrical devices to observe chaotic behavior and is shown in Fig. 13 (left). We deploy it due to its simplicity in the context of this work to mimic a conglomerate of action potentials from neuron populations. It consists of three reactive elements and an additive piecewise linear active resistor that is also known as Chua's diode whose characteristic curve is illustrated in Fig. 13 (right). Due to the piecewise linearity, this circuit is an interesting application example.

The underlying, initially nonlinear state-space model is denoted by

$$\begin{aligned}\begin{bmatrix}\dot{u}\\ \dot{v}\\ \dot{j}\end{bmatrix} &= \begin{bmatrix}-\frac{1}{C_1 R} & \frac{1}{C_1 R} & 0\\ \frac{1}{C_2 R} & -\frac{1}{C_2 R} & \frac{1}{C_2}\\ 0 & -\frac{1}{L} & 0\end{bmatrix}\begin{bmatrix}u\\ v\\ j\end{bmatrix} - \begin{bmatrix}\frac{i_{\mathrm{D}}(u)}{C_1}\\ 0\\ 0\end{bmatrix} + \begin{bmatrix}\frac{1}{C_1}\\ 0\\ 0\end{bmatrix} i,\\ y_\mu &= \begin{bmatrix}1 & 0 & 0\end{bmatrix}\begin{bmatrix}u\\ v\\ j\end{bmatrix},\end{aligned} \tag{29}$$

where

$$i_{\mathrm{D}}(u) = G_{\mathrm{b}} u + \frac{1}{2}[G_{\mathrm{a}} - G_{\mathrm{b}}][|u + u_{\mathrm{th}}| - |u - u_{\mathrm{th}}|]. \tag{30}$$

Note that both conductance values are negative, making the diode the only active element in the circuit. Due to the piecewise linearity of the diode, linearizing its characteristic curve yields valuable information about the circuits behavior. The Hartman-Grobman theorem [39] furthermore suggests that the local behavior of the nonlinear system (29) can be characterized by its linearization in the neighborhood of a hyperbolic equilibrium point. For example, the chaotic behavior known in the literature by the circuit of Fig. 13 can be explained as follows. Linearizing the diode around its conductance value in section II, such that $G_{\mathrm{NL}}(u) = G_{\mathrm{b}}$, and then checking the eigenvalues of the now linear state-space model reveals that the overall circuit is asymptotically stable. Consequently, the circuit is desired to reach the equilibrium point $u = 0$. To do so, the diode will cross the borderline between sections Ⓘ and Ⓘ𝕀. Linearizing the diode around its conductance value in section Ⓘ, such that $G_{\mathrm{NL}}(u) = G_{\mathrm{a}}$ reveals however, that in this case the diode makes the overall circuit unstable. Consequently, u grows and will cross the borderline between sections Ⓘ and Ⓘ𝕀 again. The constant crossing of the diode between sections Ⓘ and Ⓘ𝕀 is what results in the chaotic behavior which is known from the literature.

B. Linearization, Decomposition, Sufficient Condition on Synchronization

In the following we have linearized the characteristic curve of the Chua diode around the conductance value $G_{\mathrm{NL}}(u) = G_{\mathrm{b}}$ which makes the circuit unstable in order to derive a sufficient condition for the set of 6 coupled Chua oscillators as depicted in Fig. 12 (top right).

The subsystems $\mathcal{N}_\mu$ are described by

$$\begin{aligned}\begin{bmatrix}\dot{u}_\mu\\ \dot{v}_\mu\\ \dot{j}_\mu\end{bmatrix} &= \begin{bmatrix}-\frac{1}{C_1}\left[\frac{1}{R} + G_{\mathrm{b}}\right] & \frac{1}{C_1 R} & 0\\ \frac{1}{C_2} & -\frac{1}{C_2 R} & \frac{1}{C_2}\\ 0 & -\frac{1}{L} & 0\end{bmatrix}\begin{bmatrix}u_\mu\\ v_\mu\\ j_\mu\end{bmatrix} + \begin{bmatrix}\frac{1}{C_1}\\ 0\\ 0\end{bmatrix} i_\mu,\\ y_\mu &= \begin{bmatrix}1 & 0 & 0\end{bmatrix}\begin{bmatrix}u_\mu\\ v_\mu\\ j_\mu\end{bmatrix},\end{aligned}$$

where the following device parameters have been taken from [40] for simulation results

$$\begin{aligned}&L = 7.14\,\mathrm{mH}, \quad C_1 = 5.56\,\mathrm{nF}, \quad C_2 = 50\,\mathrm{nF}, \quad u_{\mathrm{th}} = 1\,\mathrm{V},\\ &G_{\mathrm{a}} = -800\,\mu\mathrm{S}, \quad G_{\mathrm{b}} = -500\,\mu\mathrm{S}, \quad R = 1.428\,\mathrm{k}\Omega.\end{aligned}$$

There, six linearized Chua circuits $\mathcal{N}_1, \ldots, \mathcal{N}_6$ are interconnected by conductances $W_{\mathrm{c}} = 5\,\mathrm{mS}$ which is the simplest model to account for the synaptic coupling strength. Note that in the case of the Chua circuit an additional capacitor in the connection element, as shown in Fig. 5 (right), will influence whether synchronization will be achieved or not. That is because both $\boldsymbol{b} = [\frac{1}{C_1} \quad 0 \quad 0]^T$ and $c^T = [1 \quad 0 \quad 0]$ only have one nonzero entry, respectively, in the first position. It follows that $\boldsymbol{C}_{\mathrm{c}}$ is matrix with only one nonzero entry in the top left position, and this entry is positive for any $C_{\mathrm{c}} > 0$, cf. (9). Consequently, the capacitance values $[C\mathbf{1}_r + \lambda_\mu\{\boldsymbol{L}\}\boldsymbol{C}_{\mathrm{c}}]$ are all positive and hence all capacitors are passive. Therefore, the interconnection conductances $\boldsymbol{W}_{\mathrm{c}}$ are of higher interest here, as they must compensate the now linearized, but still active Chua diode. This is why we focus on an interconnection network purely based on conductances here.

The conductances realize three interconnection topologies over time, most remarkable in a separated ring topology from

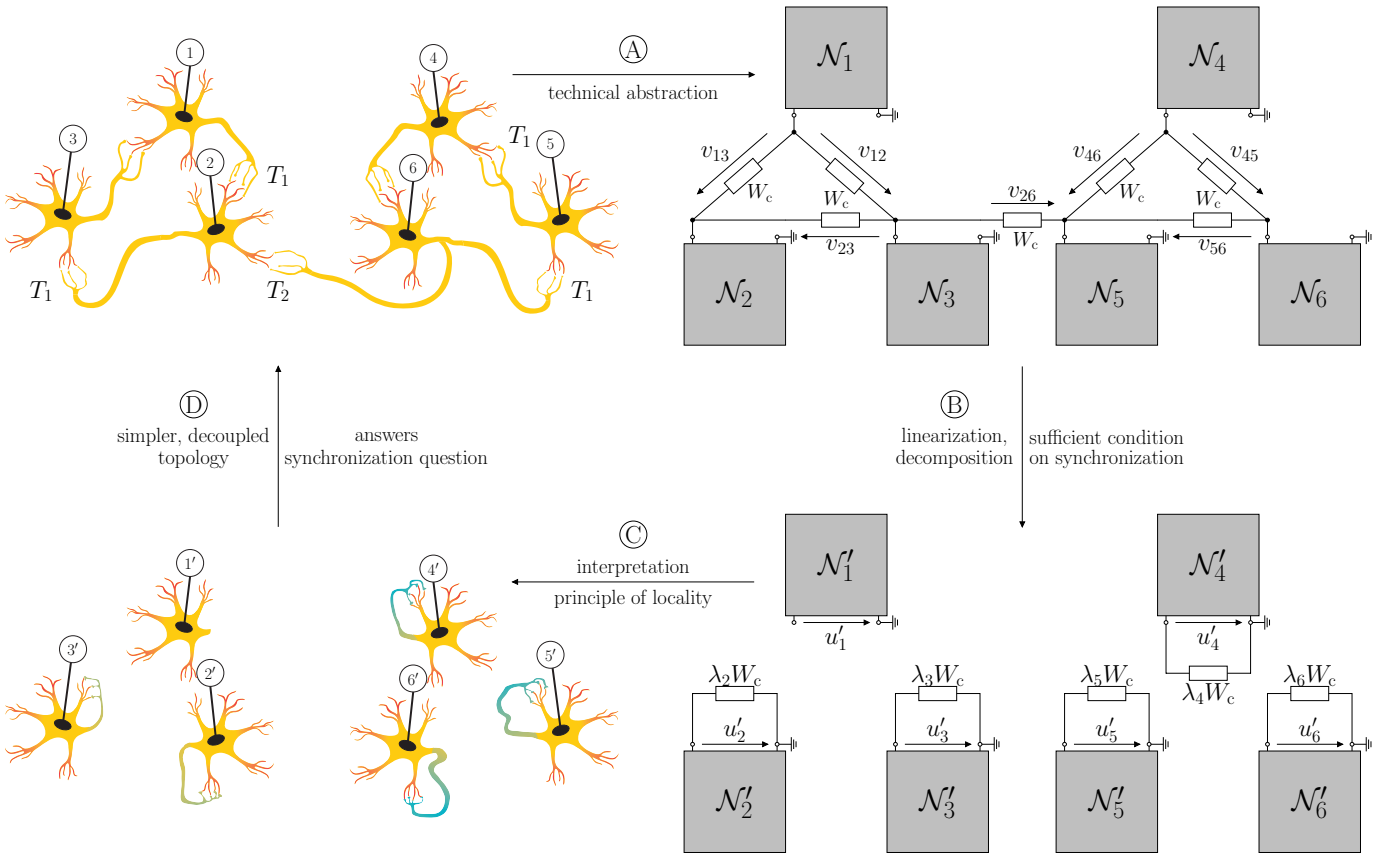

Fig. 12: Top left: Six neuron populations and their synaptic interconnections. Top right: Technical abstraction of the issue presented in the top left, where systems $\mathcal{N}_1, \ldots, \mathcal{N}_6$ each represent a neuron population and their synaptic interconnections are modeled by the resistive interconnection network. Bottom right: Decomposition approach presented in this paper yields a disconnected setup for which it is easier to determine a condition of synchronization. Bottom left: Interpretation of the decoupled setup reveals equivalent disconnected (simplified) neuron populations with only self-coupling.

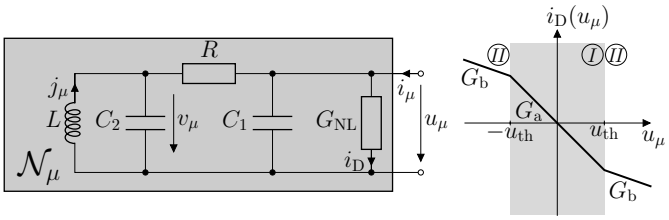

Fig. 13: Single Chua circuit with Chua's diode G_{NL} (left). Nonlinear characteristic curve of Chua's diode with its sections I and II (right).

$T_1 \leq t < T_2$ and an added bridge-synapse-like connecting the two rings from $t \geq T_2$. By a consistent notation of voltages and currents of the interconnection network in accordance with (8) and (9), we obtain

$$\boldsymbol{W}_{\mathrm{c}} = W_{\mathrm{c}} \boldsymbol{b}\boldsymbol{c}^T = \begin{bmatrix} \frac{W_{\mathrm{c}}}{C_1} & 0 & 0 \\ 0 & 0 & 0 \\ 0 & 0 & 0 \end{bmatrix}, \text{ and } \hat{\boldsymbol{W}}_\nu = \boldsymbol{L}_\nu \otimes \boldsymbol{W}_{\mathrm{c}},$$

cf. (11). We now deploy the steps described in the previous section to obtain the decoupled overall system as shown in Fig. 11, leading to

$$\begin{bmatrix} \dot{u}'_\mu \\ \dot{v}'_\mu \\ \dot{\jmath}'_\mu \end{bmatrix} = \begin{bmatrix} -\frac{1}{C_1}\left[\frac{1}{R} + G_{\mathrm{b}} + \lambda_\mu\{\boldsymbol{L}_{\boldsymbol{\nu}}\} W_{\mathrm{c}}\right] & \frac{1}{C_1 R} & 0 \\ \frac{1}{C_2 R} & -\frac{1}{C_2 R} & \frac{1}{C_2} \\ 0 & -\frac{1}{L} & 0 \end{bmatrix} \begin{bmatrix} u'_\mu \\ v'_\mu \\ \jmath'_\mu \end{bmatrix},$$

$\mu = 1, \ldots, 6,\ \nu = 0, 1, 2$. The associated decoupled system is displayed in Fig. 12 (bottom right). For the sake of a simpler asymptotic stability analysis, we summarize the linearized diode and the attached conductance $\lambda_\mu\{\boldsymbol{L}_{\boldsymbol{\nu}}\} W_{\mathrm{c}}$ of every decoupled subsystem. These are denoted by

$$W_{\mu,\nu} = G_{\mathrm{b}} + \lambda_\mu\{\boldsymbol{L}_{\boldsymbol{\nu}}\} W_{\mathrm{c}}.$$

Note that these two device are in parallel and their conductances can therefore be added to obtain a summarized conductance element. It becomes clear that the topology influences the eigenvalues of $\boldsymbol{L}_\nu$ and therefore also the values of the attached conductances of the decoupled subsystems and consequently $W_{\mu,\nu}$. Picking up on the final remark of Section V, it becomes evident that when a conductance $W_{\mu,\nu}$ is nonnegative, the according subsystem $\mathcal{N}'_\mu$ contains only passive elements and hence is asymptotically stable. This is because its admittance function can be expressed as

$$\mathcal{Y}(p) = W_{\mu,\nu} + \mathcal{Y}_0(p),$$

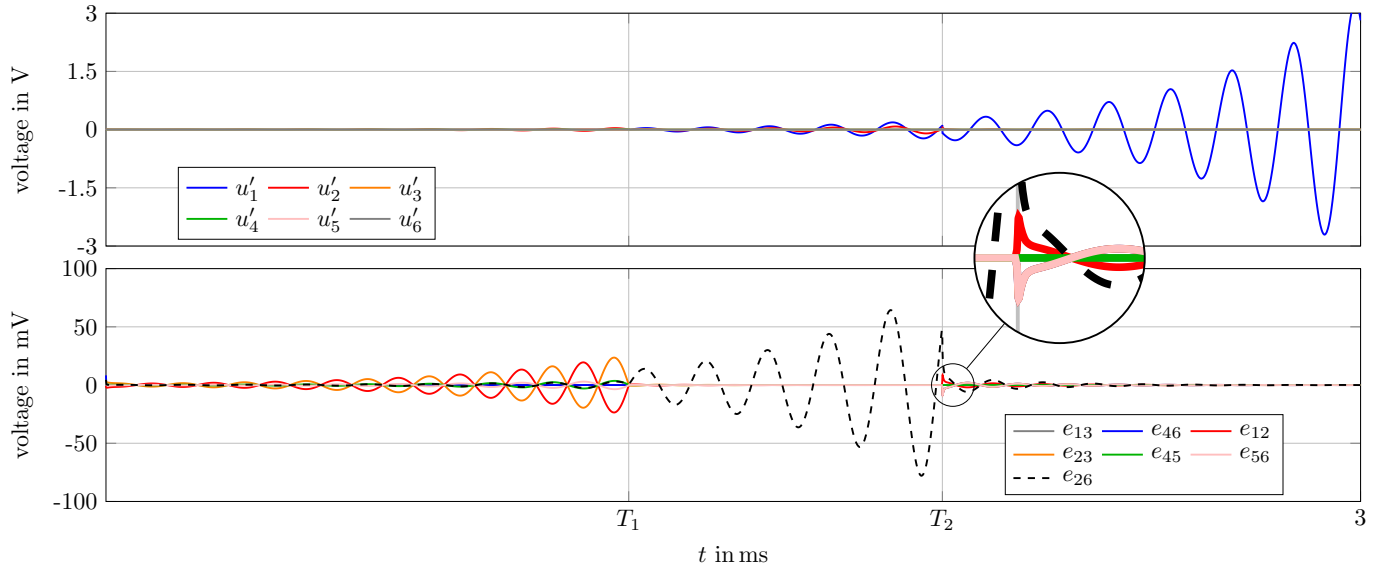

Fig. 14: Simulation results for the setup of Fig. 12 (bottom) and its synchronization errors with sparse coupling ($0 \leq t \leq T_1$), separate ring topology without ($T_1 < t \leq T_2$) and with bridge-synapse interconnection ($t > T_2$).

where $\mathcal{Y}_0(p)$ accounts for the part containing C_1, C_2, L and R, and since all elements are passive it holds that $\mathrm{Re}(p) \geq 0 \Rightarrow \mathrm{Re}(\mathcal{Y}_0(p)) \geq 0$. Hence, it follows that the circuit is asymptotically stable as $\mathrm{Re}(p) \geq 0 \Rightarrow \mathrm{Re}(\mathcal{Y}(p)) > 0$, if $W_{\mu,\nu} > 0$ holds. Specifically, $\mathrm{Re}(\mathcal{Y}_0(p)) = 0$ is reached when $p = \pm \mathrm{i}\omega_0$, where ω_0 is the resonance frequency of the oscillatory part consisting of C_2 and L. With that knowledge it is straight forward to analyze the decoupled subsystems. The simulation results of $\mathcal{N}_1, \ldots, \mathcal{N}_6$ and their respective output voltages $u_1', \ldots, u_6'$ generated with integrated circuit simulator software LTspice are shown in Fig. 14.

From $0 \leq t \leq T_1$, the Laplace matrix is

$$\boldsymbol{L}_0 = \left[\begin{array}{ccc|ccc} 1 & 0 & -1 & 0 & 0 & 0 \\ 0 & 0 & 0 & 0 & 0 & 0 \\ -1 & 0 & 1 & 0 & 0 & 0 \\ \hline 0 & 0 & 0 & 1 & 0 & -1 \\ 0 & 0 & 0 & 0 & 0 & 0 \\ 0 & 0 & 0 & -1 & 0 & 1 \end{array}\right],$$

and it can be seen that indeed $u_2', \ldots, u_4'$ are unstable as expected since $\lambda_2\{\boldsymbol{L}_0\} = \lambda_3\{\boldsymbol{L}_0\} = \lambda_4\{\boldsymbol{L}_0\} = 0$ and consequently $W_{2,0} = W_{3,0} = W_{4,0} = -800\ \mu\mathrm{S}$. Note that during this time span, only a coupling between systems $\mathcal{N}_1$ and $\mathcal{N}_3$, and $\mathcal{N}_4$ and $\mathcal{N}_6$ exist. As suggested by the course of e_{13} and e_{46}, these two pairs synchronize separately. In the following time period where $T_1 < t \leq T_2$, we have two ring topologies which are not yet connected to one another which can be seen from Fig. 12 (top left). This is indicated by the block diagonal structure of

$$\boldsymbol{L}_1 = \left[\begin{array}{ccc|ccc} 2 & -1 & -1 & 0 & 0 & 0 \\ -1 & 2 & -1 & 0 & 0 & 0 \\ -1 & -1 & 2 & 0 & 0 & 0 \\ \hline 0 & 0 & 0 & 2 & -1 & -1 \\ 0 & 0 & 0 & -1 & 2 & -1 \\ 0 & 0 & 0 & -1 & -1 & 2 \end{array}\right].$$

By calculating $W_{2,1} = -800\ \mu\mathrm{S}$ and $W_{3,1} = W_{4,1} = W_{5,1} = W_{6,1} = 14.2\ \mathrm{mS}$ we know that subsystems $\mathcal{N}_3', \ldots, \mathcal{N}_6'$ are asymptotically stable due to passivity, which is also observable in the middle part of Fig. 14. The trajectory of the synchronization errors indicate that each of the two separate ring topologies synchronize (intra-ring synchronization). Obviously, an inter-ring synchronization is not yet possible as the two rings are unlinked at this moment. This however changes when at $t = T_2$ the bridge-synapse-like connection between the rings is established. The according Laplace matrix $\boldsymbol{L}_2$ is

$$\boldsymbol{L}_2 = \left[\begin{array}{ccc|ccc} 2 & -1 & -1 & 0 & 0 & 0 \\ -1 & 3 & -1 & 0 & 0 & -1 \\ -1 & -1 & 2 & 0 & 0 & 0 \\ \hline 0 & 0 & 0 & 2 & -1 & -1 \\ 0 & 0 & 0 & -1 & 2 & -1 \\ 0 & -1 & 0 & -1 & -1 & 3 \end{array}\right],$$

and it can be seen from $W_{2,2} = 1.4\ \mathrm{mS}$, $W_{3,2} = W_{4,2} = W_{5,2} = 14.2\ \mathrm{mS}$ and $W_{6,2} = 22\ \mathrm{mS}$ that only now all subsystems $\mathcal{N}_2', \ldots, \mathcal{N}_6'$ become asymptotically stable which is observable in Fig. 14. Hence, all synchronization errors now vanish asymptotically, including e_{26}, such that inter-ring synchronization is established. One interesting observation is that the intra-ring synchronizations are temporarily broken up in order to then establish the overall synchronization.

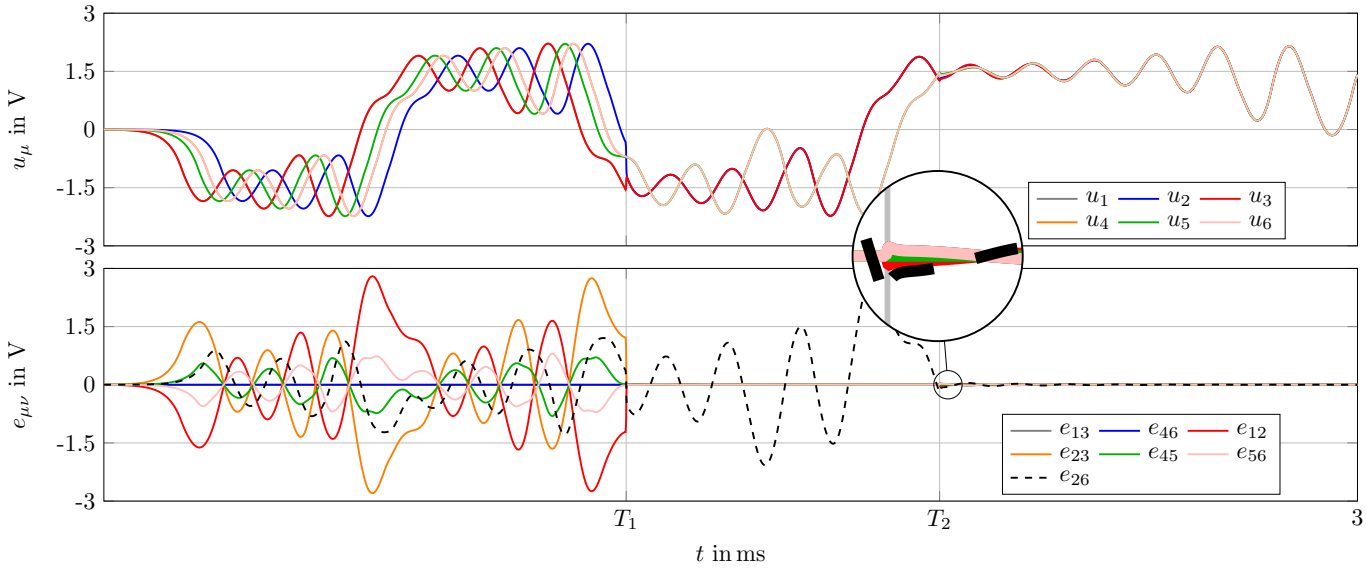

Fig. 15: Simulation results for the nonlinear setup of Fig. 12 (top) to verify the sufficient condition of synchronization with sparse coupling ($0 \leq t \leq T_1$), separate ring topology without ($T_1 < t \leq T_2$) and with bridge-synapse interconnection ($t > T_2$).

C. Interpretation, Principle of Locality

By interpreting the decomposing subsystems $\mathcal{N}_1, \ldots, \mathcal{N}_6$ into its decoupled equivalents $\mathcal{N}'_1, \ldots, \mathcal{N}'_6$, the question of synchronization can be answered easier. This becomes even more evident if we interpret the decomposition in the context of neuron populations which is done in Fig. 12 (bottom left). In the previous Section it was shown that due to the linearization, the structure of the subsystems remains invariant during the decomposition procedure. Therefore, the neuron populations are not effected, just the interconnection structure. Because the decomposition is done in a manner such that the coupling structure in diagonal, all interconnections are translated into equivalent self-couplings exclusively. We therefore are left with the same set of neuron populations with a synaptic connection to themselves. The behavior of this new set of neuron populations gives insight of the question of synchronization, but with the difference that the principle of locality is applicable here, since the neuron populations do not influence one another and can be investigated separately. Consequently, the complexity of examining synchronization in a neural network like this does not scale with the number of neuron populations but remains constant.

D. Verification of Synchronization

The final step is to showcase that the statements made for the linearized model regarding synchronization are valid for the nonlinear case as well. The simulation results for the original nonlinear system, again generated by LTspice, is shown in Fig. 15 and the following can be observed. For $0 \leq t \leq T_1$, e_{13} and e_{46} vanish, as it was for the linearized case. In the next period from $T_1 < t \leq T_2$, we also notice the intra-ring synchronization which was observable before as well. Finally, for $t > T_2$, the inter-ring synchronization is achieved asymptotically as indicated by the course of e_{26} and the intra-ring topology is temporarily disturbed in order to achieve the state of complete synchronization. A different viewpoint is provided by Fig. 16, where the trajectories of subsystems $\mu = 2$ and $\mu = 6$ are visualized. Here, the typical double attractor pattern of the chaotic Chua circuit can be observed. Furthermore, the course of e_{26} has been used as the coloring scheme for the trajectory of subsystem $\mu = 6$. It can be observed in detail what course the trajectory takes from start (indicated by the black "X") until global synchronization is achieved as indicated by the continuously green colored part at the top. In summary, the important and overriding questions regarding the synchronization behavior of the coupled nonlinear setup can be answered by the linearized and decomposed setup.

VII. Conclusion and Future Research

In this work, a generic approach for synthesis of a linear state-space model with the aim of synchronization is presented. First, the state variable has been interpreted as a voltage, leading the differential equation to represent a Kirchhoff nodal equation with capacitors and conductances as the proper electrical devices. In this context, a condensed representation of both synthesized circuits has been achieved by defining multiport circuit elements such as the multiport gyrator. Next, a step by step instruction has been presented on how a strategically smart placement of a multiport transformer can help to shift perspective in order to check decoupled subsystems for synchronization rather than a coupled overall setup. This enabled the derivation of the main contributions of this work besides the synthesis of the electrical circuits: First, a synchronization condition based on the asymptotic stability of the decoupled subsystems (rather than the coupled overall system) has been established. These decoupled subsystems are structurally identical to the coupled subsystems with the same electrical device values. They only differ in their initial conditions. Second, it has been shown that the electrical

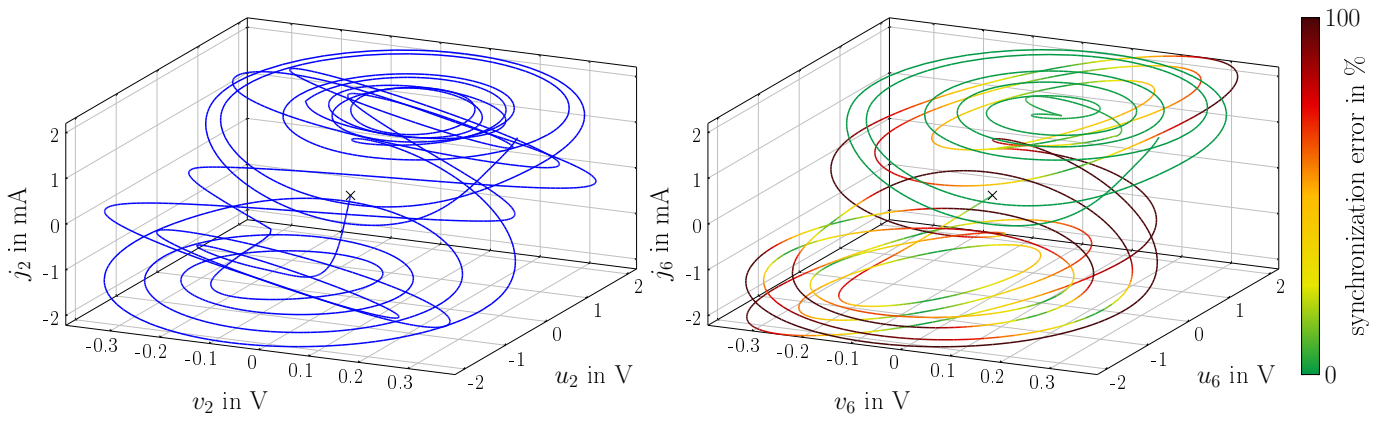

Fig. 16: Trajectories of Chua circuits $\mu = 2$ (left) and $\mu = 6$ (right) showing the typical chaotic attractor pattern. The color highlights the course of synchronization error e_{26}, where the continuously green colored trajectory on top indicates that global synchronization has been achieved.

interpretation of the synchronization condition is beneficial, since passivity of electrical devices within the circuit is easy to check without calculation. In many cases, the asymptotic stability of a circuit can be explained by the means of passivity and in those cases no calculation of eigenvalues to check for definiteness is necessary. Hence, this approach can be easier to handle compared to the classical system-theoretical approach. In the subsequent simulation scenario we have shown an example where this benefit is apparent. We have investigated a network of neuron populations with synaptic interconnections which was modeled by a set of coupled Chua circuits. We have explicitly shown how the interconnection topology affects the decoupled subsystems and how we have determined the satisfaction of the synchronization condition without calculating the eigenvalues of a system matrix.

For future research it is interesting to expand the concept of synthesizing an electrical circuit for nonlinear subsystems with possible nonlinear coupling with memory. While there exist simple electrical realizations of hybrid synapses incorporating reactive elements like capacitors and inductors [35], [41], the goal must be towards nonlinear synapses with a memory. Here, a memristor is interesting for future research since it has been shown to enable spike timing dependent plasticity [42]. That however will require a modified approach, as the decoupling of the subsystems will not be successful in the nonlinear case with the concept presented in this work. Additionally, it might be interesting to allow the interconnections between subsystems to be described by differential equations, as for example in [43]. That would enable the derivation of a generic approach on how to synthesize and analyze neuromorphic applications, such as neuron populations with Hebbian learning rule or spike timing dependent plasticity.

Acknowledgments

The financial support by the German Research Foundation (Deutsche Forschungsgemeinschaft - DFG) through FOR 2093 and DFG-404291403 is gratefully acknowledged.

References

[1] A. K. Engel, P. Fries, and W. Singer, "Dynamic predictions: Oscillations and Synchrony in top-down Processing," *Nat. Rev. Neurosci.*, vol. 10, no. 2, pp. 704–716, Oct. 2001.

[2] W. Singer, "Synchronization of Cortical Activity and its Putative Role in Information Processing and Learning," *Annual Review of Physiology*, vol. 55, pp. 349–374, 1993.

[3] V. N. Murthy and E. E. Fetz, "Oscillatory Activity in Sensorimotor Cortex of awake Monkeys: Synchronization of local Field Potentials and Relation to Behavior," *Journal of Neurophysiology*, vol. 76, no. 6, pp. 3949–67, Dec. 1996.

[4] F. G. Andres and C. Gerloff, "Coherence of Sequential Movements and Motor Learning," *Journal of Clinical Neurophysiology*, vol. 16, no. 6, pp. 520–7, Dec. 1999.

[5] K. Ochs and D. Michaelis, "Mimicking Gait Pattern Generators," *61st IEEE Midwest Symposium on Circuits and Systems, Windsor, Canada*, Aug. 2018.

[6] A. Mosebach and J. Lunze, "A Deterministic Gossiping Algorithm for the Synchronization of Multi-Agent Systems," *5th IFAC Workshop on Distributed Estimation and Control in Networked Systems (NecSys)*, pp. 1–7, Sep. 2015.

[7] G. B. Ermentrout, "The behavior of rings of coupled oscillators," *Journal of Mathematical Biology*, vol. 23, no. 1, pp. 55–74, Dec. 1985.

[8] Y. Nishio and A. Ushida, "On a Ring of Chaotic Circuits Coupled by Inductors," *IEICE Trans. FUndamentals*, vol. E78, no. 5, pp. 608–617, May 1995.

[9] Y. Kuramoto, "Self-Entrainment of a Population of Coupled Non-linear Oscillators," *Lecture Notes in Physics*, vol. 39, no. 1, Jan. 1975.

[10] K. Ochs, D. Michaelis, and J. Roggendorf, "Circuit Synthesis of the Kuramoto Model and Electrical Interpretation of its Synchronization Condition," *2019 DPG-Frühjahrstagung Aachen*, Mar. 2019.

[11] L. O. Chua, "Chua's Circuit: An Overview Ten Years Later," *Journal of Circuits, Systems and Computers*, vol. 4, no. 2, pp. 117–159, 1994.

[12] P. Feketa, A. Schaum, T. Meurer, D. Michaelis, and K. Ochs, "Synchronization of nonlinearly coupled networks of Chua oscillators," *11th IFAC Symposium on Nonlinear Control Systems, Vienna, Austria*, pp. 1103 – 1108, Sep. 2019.

[13] E. Bilotta, S. Gervasi, and P. Pantano, "Reading Complexity in Chua's Oscillator Through Music. Part I: A New Way of understanding chaos, International Journal of Bifurcation and Chaos," *International Journal of Bifurcation and Chaos*, vol. 15, no. 2, pp. 253–382, Aug. 2005.

[14] E. Bilotta and P. Pantano, "The Language of Chaos," *International Journal of Bifurcation and Chaos*, vol. 16, no. 3, pp. 523–557, 2006.

[15] T. Yang and L. Chua, "Impulsive stabilization for control and synchronization of chaotic systems: theory and application to secure communication," *IEEE Transactions on Circuits and Systems I: Fundamental Theory and Applications*, vol. 44, no. 10, pp. 976–988, Oct. 1997.

[16] J. Ohtsubo, "Chaos synchronization and chaotic signal masking in semiconductor lasers with optical feedback," *IEEE Journal of Quantum Electronics*, vol. 38, no. 9, pp. 1141–1154, Sep. 2002.

[17] E. Panaintescu, A. Carlucci Rezende, and M. Stoicescu, "Chua Circuit as Cognitive Dynamical System," *Physics AUC*, vol. 23, pp. 55–62, 2013.

[18] L. V. Gambuzza, M. Frasca, and V. Latora, "Distributed Control of Synchronization of a Group of Network Nodes," *IEEE Transactions on Automatic Control*, vol. 64, no. 1, pp. 365–372, Jan. 2019.

[19] K. Ochs and D. Michaelis, "Neural Network Topology Formation Using Memristive Jaumann Structures," *61st IEEE Midwest Symposium on Circuits and Systems, Windsor, Canada*, Aug. 2018.

[20] I. Belykh, E. de Lange, and M. Hasler, "Synchronization of Bursting Neurons: What Matters in the Network Topology," *Physical Review Letters*, vol. 94, no. 18, p. 188101, Jun. 2005.

[21] J. Fell and N. Axmacher, "The Role of Phase Synchronization in Memory Processes," *Nature Reviews Neuroscience*, vol. 12, no. 2, pp. 105–18, Feb. 2011.

[22] A. Schnitzler, C. Münks, M. Butz, L. Timmermann, and J. Gross, "Synchronized Brain Network associated with Essential Tremor as revealed by Magnetoencephalography," *Movement Disorders*, vol. 24, no. 11, pp. 1629–35, 2009.

[23] R. K. Wong, R. D. Traub, and R. Miles, "Cellular Basis of Neuronal Synchrony in Epilepsy," *Advances in Neurology*, vol. 44, pp. 583–92, 1986.

[24] C. Hammond, H. Bergman, and P. Brown, "Pathological synchronization in Parkinson's Disease: Networks, Models and Treatments," *Trends in Neurosciences*, vol. 30, no. 7, pp. 357–364, Jul. 2007.

[25] K. Ochs, D. Michaelis, and E. Solan, "Towards Wave Digital Memcomputing With Physical Memristor Models," *IEEE Transactions on Circuits and Systems I: Regular Papers*, pp. 1–11, 2019.

[26] F. L. Traversa and M. Di Ventra, "Polynomial-time Solution of Prime Factorization and NP-hard Problems with Digital Memcomputing Machines," *Chaos: An Interdisciplinary Journal of Nonlinear Science*, vol. 27, no. 2, p. 023107, 2017.

[27] K. Ochs, E. Solan, D. Michaelis, and M. Herbrechter, "Towards Wave Digital Memcomputing with Physical Memristor Models," *52nd IEEE International Symposium on Circuits and Systems, Sapporo, Japan*, pp. 1 – 4, May 2019.

[28] M. Ziegler, K. Ochs, M. Hansen, and H. Kohlstedt, "An electronic Implementation of Amoeba Anticipation," *Applied Physics A*, vol. 114, no. 2, pp. 565–570, 2013.

[29] K. Ochs, M. Ziegler, E. Hernandez-Guevara, E. Solan, M. Ignatov, M. Hansen, M. S. Gill, and H. Kohlstedt, "Anticipation of digital patterns," *International Journal of Circuit Theory and Applications*, vol. 46, no. 2, pp. 235–243, 2018.

[30] A. Fettweis, "Wave digital filters: Theory and practice," *Proceedings of the IEEE*, vol. 74, no. 2, pp. 270–327, Feb. 1986.

[31] K. Meerkötter, "On the Passivity of Wave Digital Networks," *IEEE Circuits and Systems Magazine*, vol. 18, no. 4, pp. 40–57, 2018.

[32] E. Solan and K. Ochs, "Wave Digital Emulation of general Memristors," *International Journal of Circuit Theory and Applications*, pp. 1–17, Jul. 2018.

[33] E. Solan, E. Perez, D. Michaelis, C. Wenger, and K. Ochs, "Wave Digital Emulation of a TiN/Ti/HfO_2/TiN RRAM Cell based on a Semi-Physical Model," *Int. J. Numer. Model.*, pp. 1–12, Mar. 2019.

[34] K. Ochs and E. Solan, "Sensitivity Analysis of Memristors based on Emulation Techniques," *IEEE 59th International Midwest Symposium on Circuits and Systems, Abu Dhabi, UAE*, pp. 1 – 4, Oct. 2016.

[35] J. Ma, Z.-q. Yang, L.-j. Yang, and J. Tang, "A physical view of computational neurodynamics," *Journal of Zhejiang University-SCIENCE A*, vol. 20, no. 9, pp. 639–659, Sep. 2019.

[36] C. W. Wu, *Synchronization in Complex Networks of Nonlinear Dynamical Systems*. World Scientific Pub Co Inc, Feb. 2007.

[37] J. Lunze, *Networked Control of Multi-Agent Systems*. Bookmundo Direct, 2019.

[38] K. Xu *et al.*, "Synchronization transition in neuronal networks composed of chaotic or non-chaotic oscillators," *Scientific Reports*, vol. 1, no. 8, p. 8370, May 2018.

[39] J. Pralis and W. de Melo, *Geometric Theory of Dynamical Systems*. Springer-Verlag New York, 1982.

[40] M. Kennedy, "Robust op amp realization of chua's circuit," *Frequenz*, vol. 46, 08 1994.

[41] C. Wang, J. Tang, and J. Ma, "Minireview on signal exchange between nonlinear circuits and neurons via field coupling," *The European Physical Journal Special Topics*, vol. 228, no. 10, pp. 1907–1924, Oct. 2019.

[42] K. Ochs, E. Hernandez-Guevara, and E. Solan, "Wave digital emulation of spike-timing dependent plasticity," in *2017 IEEE 60th International Midwest Symposium on Circuits and Systems (MWSCAS)*, vol. 1558-3899 (ISSN). Boston, MA, USA: IEEE, Aug. 2017, pp. 152–155.

[43] P. Feketa, A. Schaum, and T. Meurer, "Synchronization and multi-cluster capabilities of oscillatory networks with adaptive coupling," *arXiv:1912.03922 [cs, eess, math]*, Dec. 2019, arXiv: 1912.03922.